A Broadband Low-Profile Dual-Polarized Antenna Based on a Metasurface

Xiwang DAI^{1,2}, Junshi ZHAO¹, Zhuoyu SHEN¹, Hui HONG¹, Gang LI³

School of Electronic Informations, Hangzhou Dianzi University, Hangzhou, China
 State Key Laboratory of Millimeter Waves, Southeast University, Nanjing, 210096, China
 Hubei Key Laboratory of Low Dimensional Optoelectronic Materials and Devices, Hubei University of Arts and Science, Xiangyang, 441053, China

xwdai@hdu.edu.cn, zjs@hdu.edu.cn, 1339079907@qq.com, hongh@hdu.edu.cn, ligang_hbuas@vip.163.com

Submitted May 15, 2025 / Accepted September 8, 2025 / Online first October 21, 2025

Abstract. This article presents a wideband low-profile dualpolarization antenna based on a metasurface (MS). The antenna consists of a 4×4 metasurface array made up of 16 circular metal patches, a radiating patch, and a metallic ground plane. The metasurface excites the surface waves of the radiating patch to generate multiple resonant points, thereby broadening the antenna bandwidth. In addition, two rectangular cross-slot structures at the center of the patch enhance port isolation. Finally, a prototype with dimensions of 46 mm \times 46 mm \times 3.2 mm (1.28 $\lambda_0 \times$ 1.28 $\lambda_0 \times$ 0.88 λ_0) was fabricated. Measurement results show that the antenna achieves a return loss better than -10 dB and an isolation better than -16 dB within the operating bandwidth of 6.38–10.3 GHz. It can be concluded that the experimental results of the antenna are in good agreement with the simulation results.

Keywords

Dual-polarization, metasurface, low-profile, broadband

1. Introduction

This dual-polarized microstrip patch antennas are a widely adopted antenna design in the fields of wireless communication and microwave technology [1], [2]. Thanks to their remarkable performance in mitigating multipath fading and enhancing channel capacity, these antennas have found extensive applications in various areas, including base station construction, Bluetooth devices, and mobile communication terminals [3], [4]. With their compact structure, ease of fabrication, and high integrability with other systems, microstrip patch antennas have gradually become the mainstream choice in the development of compact antennas [5–9]. However, the inherent narrow bandwidth and low gain of microstrip patch antennas still restrict their use in certain scenarios with extremely high performance requirements, especially in complex communication environments where broadband coverage and high gain are explicitly demanded, where these limitations are particularly pronounced [2], [8].

To address the inherent narrow bandwidth of patch antennas, several methods to enhance bandwidth have been developed up to now. The Fabry-Perot cavity method can effectively increase the antenna's gain and bandwidth [10], [11]. Antennas using multilayer stacked substrates and parasitic patches can effectively broaden the antenna impedance bandwidth by achieving multiple resonant points [12], [13]. Slot structures [14], [15] and probe structures [16–18] can also be employed to improve the impedance bandwidth. However, these antennas have the disadvantages of complexity and high profile, and these structural designs will reduce the mechanical performance of the antenna and increase the antenna processing cost.

To overcome the aforementioned drawbacks, this paper proposes a broadband, low-profile dual-polarized antenna based on a metasurface. The antenna employs a threelayer composite structure: the top layer is a 4×4 circular patch metasurface array (16 elements) to extend the bandwidth; the middle layer features a circular radiating patch with dual rectangular slots etched at the center to significantly enhance port isolation, and four fan-shaped slots and rectangular trapezoidal composite microstrip lines are introduced to optimize impedance matching. The measured results show that this antenna, with dimensions of only 46 mm \times 46 mm \times 3.2 mm (1.28 $\lambda_0 \times$ 1.28 $\lambda_0 \times$ 0.088 λ_0), achieves excellent performance: an impedance bandwidth of 6.38–10.3 GHz (relative bandwidth of 47.1%) with a return loss of less than -10 dB, a 3-dB gain bandwidth covering 6.28-9.98 GHz (45.51%), and a peak broadside gain of 6.45 dB at 7.38 GHz.

2. Antenna Design and Performances

2.1 Antenna Element

Figure 1 illustrates the overall structure of the proposed broadband, low-profile dual-polarized antenna based on a metasurface. The top layer consists of a 4×4 circular metallic patch array metasurface printed on the upper surface of the FR4 dielectric substrate 2 (with a period of P, patch

DOI: 10.13164/re.2025.0641

diameter of CR2, and unit spacing of S1) [19]. The middle layer is the radiating patch sandwiched between two dielectric substrates, featuring four fan-shaped and rectangular interdigital slots etched on the circular metallic patch. The bottom layer is the metallic ground plane. The antenna adopts a dual-feed design, feeding the driven patch through coaxial lines passing through the dielectric layer. Both probe feed points are located at the circular slot of the T-shaped microstrip line, with port matching adjusted via the T-shaped transmission structure. The inner conductor of the coaxial line is soldered to the T-shaped microstrip line through the circular slot on it, thereby achieving antenna excitation [2]. This compact stacked structure (metasurface-dielectric substrate 2–radiating patch–dielectric substrate 1–ground plane) realizes broadband, low-profile, and dual-polarization characteristics.

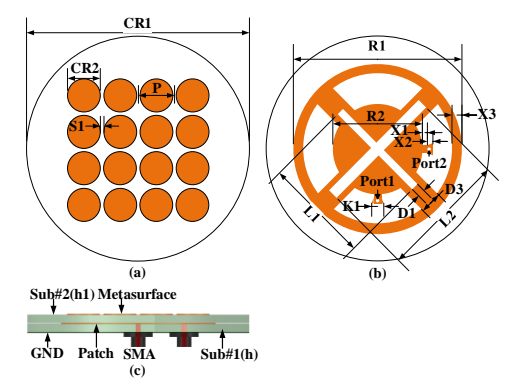


Fig. 1. Geometry of the proposed antenna: (a) Top view of the metasurface. (b) Top view of the driven patch. (c) Side view

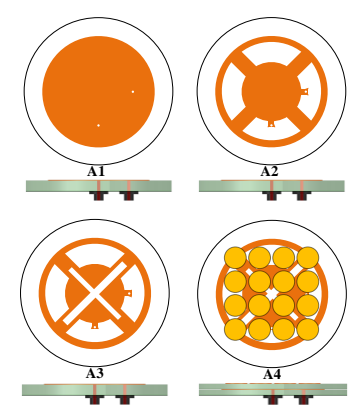


Fig. 2. Proposed antennas in different configurations.

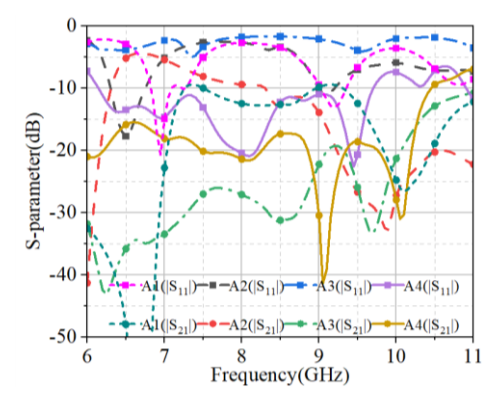


Fig. 3. S-parameters of antennas with different structures.

Optimization of the antenna using HFSS resulted in a dual-polarized antenna with a wide impedance bandwidth and high isolation. The optimized design parameters are: CR1 = 46 mm, CR2 = 6.8 mm, P = 7.55 mm, S1 = 0.75 mm, R1 = 32 mm, R2 = 17 mm, L1 = 20 mm, L2 = 24 mm, D1 = 1.4 mm, D2 = 2 mm, D3 = 4.2 mm, X1 = 0.8 mm, X2 = 1.25 mm, X3 = 2 mm and K1 = 2.5 mm.

2.2 Design Methodology

The design methodology of the proposed circular patch antenna is structured to provide a systematic approach for determining the initial geometric parameters and achieving optimized performance at the target operating frequency. The key steps are outlined as follows:

1) Substrate Selection and Target Frequency Definition

To reduce fabrication costs while maintaining acceptable performance, FR4 is selected as the dielectric substrate. The antenna is designed to operate at a center frequency of 8 GHz. The relative permittivity ε_r of FR4, typically around 4.4, plays a crucial role in determining the physical dimensions of the radiating patch.

2) Initial Radius Estimation of the Circular Patch

The resonant frequency of the circular microstrip patch is governed by the TM_{nm} mode. For initial estimation of the patch radius a, the following equation is used:

$$a = \frac{F}{\sqrt{\varepsilon_{\rm r}}}$$
 where $F = \frac{8.791 \times 10^9}{f_{\rm r} \sqrt{\varepsilon_{\rm eff}}}$. (1)

Here, f_r is the target resonant frequency, and $\varepsilon_{\rm eff}$ is the effective dielectric constant, which accounts for fringing fields.

3) Verification via Resonant Frequency Formula

The calculated radius is validated using the TM_{nm} mode resonance condition:

$$f_{nm} = \frac{\chi_{nm} \cdot c}{2\pi a \sqrt{\varepsilon_{\text{eff}}}} \tag{2}$$

where χ_{nm} is the *n*-th root of the derivative of the *m*-th order Bessel function, and *c* is the speed of light in free space. In simulation, a patch radius of 16 mm excites the TM₃₁ mode, resonating at 6.9 GHz, validating the analytical model.

4) Impedance Matching and Bandwidth Enhancement

To improve port matching and enhance impedance bandwidth, several structural modifications are introduced:

- Four sector-shaped slots are etched symmetrically in the circular patch.
- A T-shaped feed structure is applied to optimize energy coupling to the radiating element.
- A central cross-shaped slot is embedded to enhance isolation and reduce mutual coupling effects.

5) Bandwidth Expansion Using Metasurface Integration

To further improve the antenna bandwidth, a metasurface layer comprising 16 circular patches arranged in a 4×4

array is printed on the top surface of the upper dielectric layer. This metasurface interacts constructively with the radiating element, resulting in significant bandwidth enhancement.

6) Final Optimization

After the initial geometry is determined using analytical and empirical models, the complete antenna structure undergoes full-wave electromagnetic simulation-based optimization. This refinement step ensures optimal resonance behavior, impedance matching, and radiation characteristics.

2.3 Performance and Operation Mechanism

In order to illustrate the performance of the aforementioned antenna and explain its working principle, we conducted a structural comparison of antennas with different configurations during the design process. As shown in Fig. 2, A1, A2, and A3 are all composed of an antenna radiating patch, a dielectric substrate, and a metallic ground layer. A1 is a circular patch, A2 is a circular patch with four fan-shaped slots and a T-shaped feed line, without a metasurface. A3 is A2 with a rectangular cross-slot etched in the center, also without a metasurface. A4 is the proposed antenna, which is based on A3 with the addition of a metasurface structure. All the antenna designs in Fig. 2 have the same overall dimensions, the same height, and the same type of dielectric substrate, and are fed by two circular slots on the lower and right sides of the circular patch to connect the coaxial line. The four antennas were simulated using HFSS, and the performance parameters are shown in Fig. 3.

As shown in Fig. 3, the S11 bandwidth of A1 is 6.82 to 7.09 GHz (with a relative bandwidth of 3.8%). The S11 bandwidth of A2 is 6.31–6.75 GHz (with a relative bandwidth of 6.7%), and it has poor port isolation. A3 achieves a significant improvement in port isolation, A4 (with the complete metasurface structure), by exciting surface waves in the metasurface to generate multiple resonance points, achieves an S11 of less than –10 dB within the frequency range of 6.16–9.68 GHz (relative bandwidth of 44%), while the port isolation is enhanced to below –15 dB across the entire passband.

In the proposed antenna, the employed metasurface is referred to as a RIS structure [19], which is composed of circular metallic lattices printed on a dielectric substrate. To reduce the antenna height, the driven patch of the antenna is positioned between the ground plane and the metasurface. The microstrip patch antenna using the metasurface has achieved a significant increase in bandwidth. This phenomenon can be regarded as the effect of surface wave propagation in the finite-sized RIS-based antenna [20], that is, the radiating system will generate additional resonances at specific frequencies, thereby improving the antenna performance. As shown in Fig. 4, the antenna without a metasurface and the antenna with a 3×3 metasurface array only have resonance near 7.5 GHz. The antenna with a metasurface array of size 4×4 or larger generates three resonance frequencies. This demonstrates that the surface waves propagating on the metasurface are excited and produce additional resonances for the antenna system. It can be said that the resonance at 7.5 GHz is generated by the driven patch, while the additional resonances caused by the surface waves occupy the high-frequency region. For the 4×4 unit structure, the two resonance frequencies are 8.1 GHz and 8.6 GHz. For the 5×5 unit structure, they are 8.2 GHz and 8.7 GHz. For the 6×6 unit structure, they are 7.7 GHz and 8.3 GHz. Therefore, the resonances caused by TM and TE surface waves can be approximately defined as the third and fourth resonance frequencies of the proposed antenna. These results show that the additional resonances are mainly determined by the number of units and can be used to improve the performance of the antenna. As shown in Fig. 5, when the unit structure is 4×4 , the performance of S_{11} is the best, so the metasurface with a 4×4 unit structure is chosen. Table 1 summarizes the comparison of performance parameters of the three antennas under different configurations.

Antenna Structure	$S_{11} \leq -10 \text{ dB}$ $BW(\%)$	$S_{21} \leq -15 \text{ dB}$ $BW(\%)$	
A1	6.82–7.09 GHz 3.8%	4.89–7.11 GHz 37%	
A2	6.31–6.75 GHz 6.7%	5.38–6.23 GHz 14.64%	
A3	-	5.48–10.32 GHz 61.27%	
A4	6.16–9.68 GHz 44.44%	3.28–10.28 GHz 103.24%	

Tab. 1. Comparison of antenna performance for different configurations.

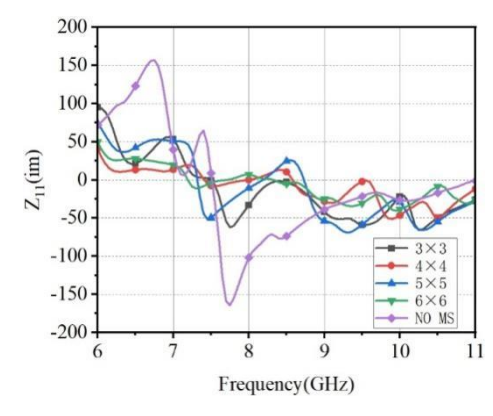


Fig. 4. The imaginary part of Z_{11} under different unit cell structures.

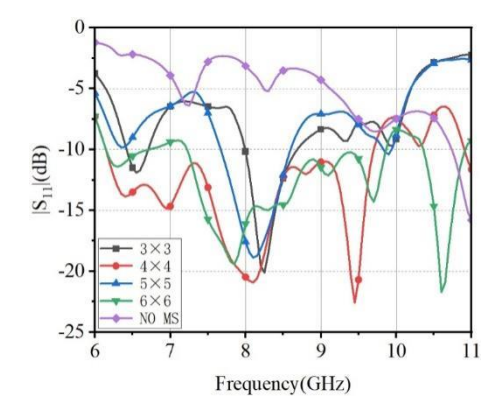


Fig. 5. The $|S_{11}|$ parameter under different unit cell structures.

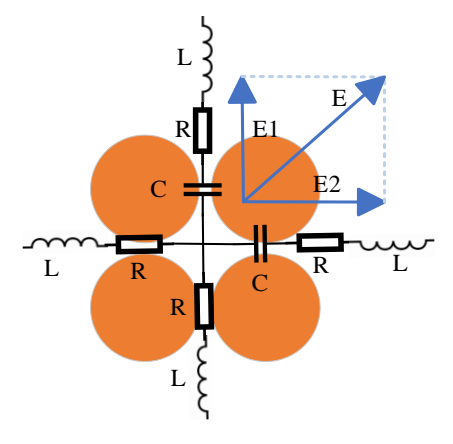


Fig. 6. Equivalent circuit of metasurface.

From the perspective of equivalent circuits, if the metasurface is excited in a specific direction and exhibits structural symmetry in the two orthogonal components of the excitation direction, then two equivalent impedances with the same amplitude and phase can be generated [21]. This allows two electric field components with the same amplitude and phase to be excited in the two orthogonal directions, resulting in the synthesis of a linearly polarized wave, as shown in Fig. 6. Considering the excitation along the E direction, due to the symmetry of the metasurface structure in both directions, the equivalent impedances along the orthogonal components E1 and E2 are equal, which can be represented as:

$$Z_1 = Z_2 = 2R + j\omega(2L) + \frac{1}{j\omega C} = |Z_1| \angle \varphi = |Z_2| \angle \varphi \quad (3)$$

where R and L are the equivalent resistance and inductance of the metasurface element along E_1 and E_2 , respectively, and C is the equivalent capacitance between the gaps of the two elements along E_1 and E_2 . Therefore, two electric field components with the same amplitude and phase can be obtained in the directions of E_1 and E_2 , respectively, thus allowing the synthesis of a linearly polarized wave.

The working principle of the antenna is further clarified by examining the current distribution on the antenna. The surface current distributions at three bandwidth extreme points (6.9 GHz, 8.1 GHz, and 9.4 GHz) are shown in Fig. 7 to 9, respectively.

The current distribution analysis in Fig. 7 to Fig. 9 reveals the working principle of the antenna: At the three S_{11} minimum points of 6.9 GHz, 8.1 GHz, and 9.4 GHz, the current distribution is observed to exhibit regular variations with the phase angle $(0^{\circ}/90^{\circ}/180^{\circ}/270^{\circ})$. At 0° , the current is concentrated at the lower right corner of the patch and on the annular microstrip line, while at 90° , the current shifts to the port connection area. Corresponding mirror distributions are observed at 180° and 270° . This characteristic indicates that the metasurface can excite two orthogonal modes, and the difference between the characteristic angles of the two orthogonal modes is 180° . These differences meet the conditions for generating horizontal or vertical (X/Y direction) linearly polarized waves [21].

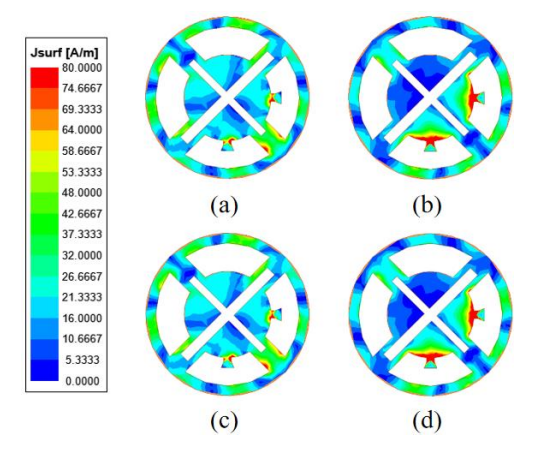


Fig. 7. Electric current distribution on the patch at 6.9 GHz: (a) 0° . (b) 90° . (c) 180° . (d) 270° .

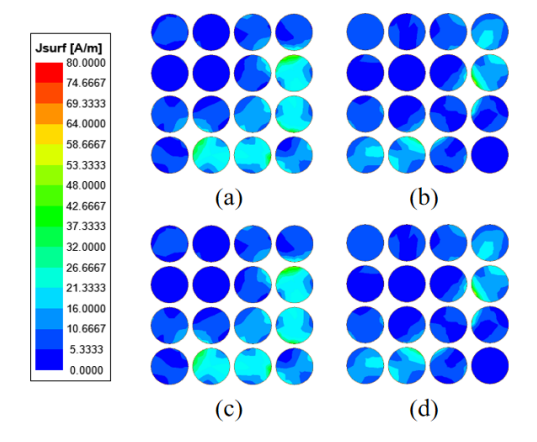


Fig. 8. Electric current distribution on the patch at 8.1 GHz: (a) 0° . (b) 90° . (c) 180° . (d) 270° .

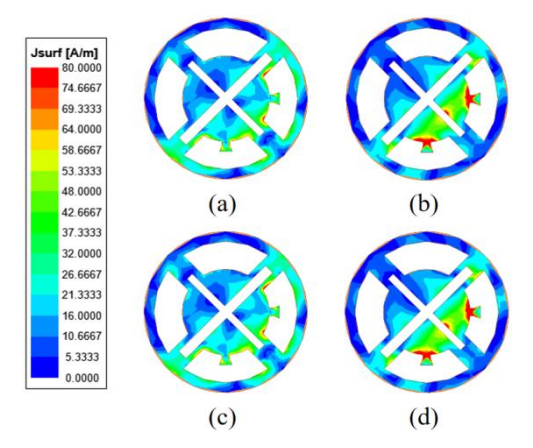


Fig. 9. Electric current distribution on the patch at 9.4 GHz: (a) 0° . (b) 90° . (c) 180° . (d) 270° .

3. Results and Discussion

To verify the performance of the proposed antenna, a physical prototype was fabricated and tested. The fabricated sample is shown in Fig. 10, where Figure 10(a) shows the radiating patch, Figure 10(b) shows the metasurface, and Figure 10(c) shows the radiating patch and metasurface fastened together with nylon screws.

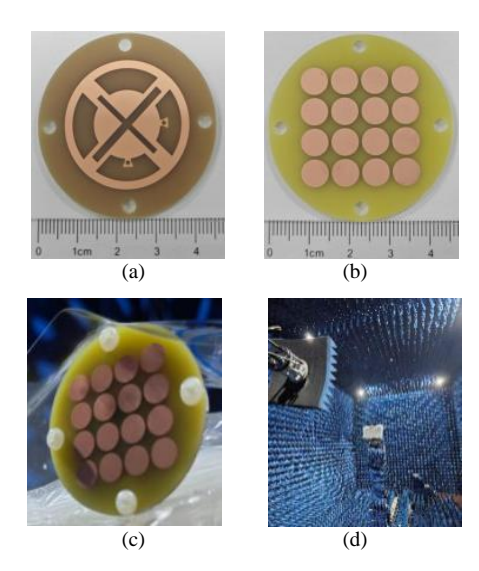


Fig. 10. Proposed antennas in different configurations.

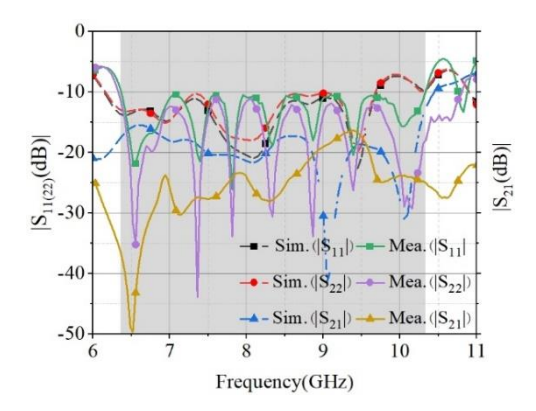


Fig. 11. S-parameter measurement comparison.

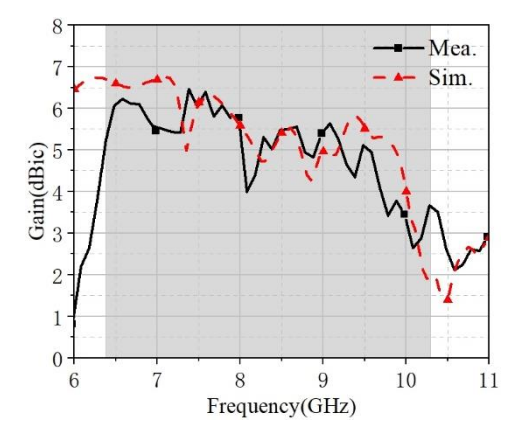


Fig. 12. Gain measurement comparison.

3.1 S-Parameter

In accordance with the S-parameter measurement procedure, the reflection coefficient of the fabricated antenna was obtained using a vector network analyzer and a 3.5 mm coaxial calibration standard (GCS35M). As shown in Fig. 11, the measured impedance bandwidth is 6.38–10.3 GHz (47.1%). The isolation between the two ports was measured to be greater than 16.4 dB. Since the metasurface and the radiating patch are fastened with nylon

screws, there must be a slight air gap between the two dielectric layers. This causes the microstrip patch and the metasurface of the antenna to produce multiple resonances together, thereby creating multiple resonant points and increasing the antenna's impedance bandwidth [2]. Therefore, the measurement results are basically consistent with the simulation results, verifying the correctness of the antenna design.

3.2 Broadside Gain

The far-field radiation pattern of the target antenna was measured in a microwave anechoic chamber at Hangzhou Dianzi University, with dimensions of 10 m (L) $\times 5 \text{ m}$ (W) $\times 7 \text{ m}$ (H). During the measurement process, waveguides covering various frequency ranges were utilized to measure and record the gain and radiation pattern of the target antenna. The measured gain of the proposed antenna is depicted in Fig. 12. In Fig. 12, the measured gain bandwidth ranges from 6.28 to 9.98 GHz, with a bandwidth of 45.51% and a peak gain of 6.45 dBic. There is some deviation from the simulated gain. These minor parameter fluctuations are due to the fact that the two dielectric substrates are fixed by screws in a stacked manner, and the two substrates are not perfectly aligned during the stacking process.

3.3 Radiation Patterns

Due to the antenna symmetry, the E-plane and H-plane radiation patterns of Port 1 and Port 2 are similar. Therefore, only the radiation patterns in the xoz plane are shown in Fig. 13. Considering repetition, Figure 13 only displays the radiation patterns in the xoz plane. It can be seen that the measured co-polarization results match well with the simulated results. As shown in Fig. 13, the cross-polarization levels measured on the E-plane and H-plane are less than $-19.04 \, \mathrm{dB}$ and $-5.69 \, \mathrm{dB}$, respectively.

4. Performance Comparison

In Tab. 2, our design is comprehensively compared with other patch antennas. Evidently, the patch antennas in [7] and [8] are all single-polarized and exhibit high-gain characteristics. However, compared to the proposed antenna, the proposed antenna demonstrates a higher S₁₁ bandwidth (BW), which provides superior impedance matching performance in broadband communication systems. Although the antennas in [22], [23], and [24] are all dual-polarized and achieve high gain, the proposed antenna not only achieves a broader bandwidth but also features a more compact size, making it more suitable for modern wireless communication devices that demand miniaturized antennas. The results indicate that this antenna combines the advantages of wide bandwidth, low profile, compatibility with dual-polarization applications, and a simple structure. It not only meets the requirements of multi-band communication systems but also reduces manufacturing complexity.

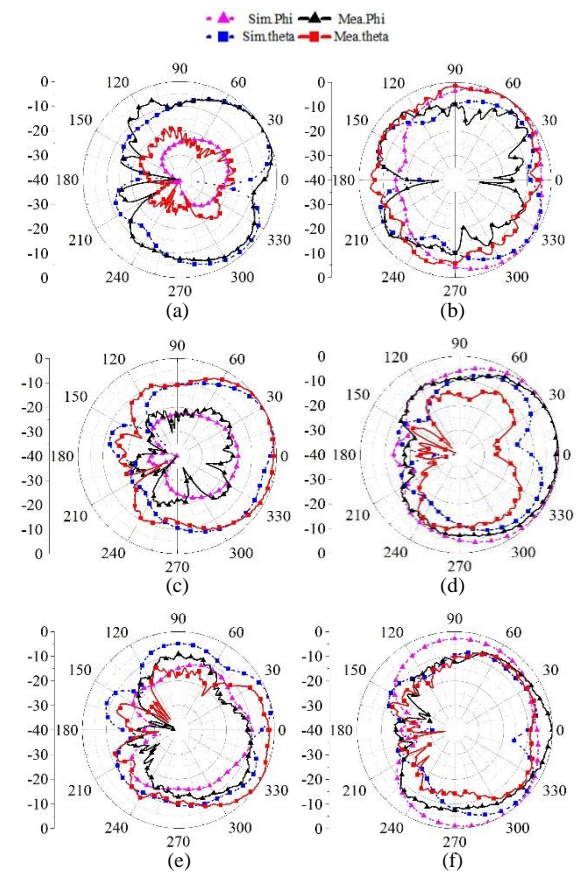


Fig. 13. Simulated and measured normalized radiation patterns of two ports in the xoz plane. Port 1 (H-plane): (a) 7.3, (c) 8.4, (e) 9.5 GHz. Port 2 (E-plane): (b) 7.3, (d) 8.4, (f) 9.5 GHz.

Antenna Structure	Size (λ_0^3)	$S_{11} \leq -10 \text{ dB}$ $BW(\%)$	Gain (dBic)
Ref. [7]	$1.6\times1\times0.075$	40	10
Ref. [8]	$0.87\times0.87\times0.06$	29	10.6
Ref. [22]	$1.65\times1.65\times0.04$	3.0	11.5
Ref. [23]	$2.50 \times 1.78 \times 0.097$	12	8.57
Ref. [24]	$1.30 \times 1.30 \times 0.049$	6.0	9.6
Proposed	$1.28\times1.28\times0.088$	47.1	6.45

 λ_0 is the free space wavelength referring to the antenna center frequency.

Tab. 2 Comparison with previously published designs.

5. Conclusion

A metasurface dual-polarization antenna with wide bandwidth, high isolation, and low profile has been proposed. A metasurface is printed on the top layer of the dielectric substrate to enhance the antenna's overall bandwidth. The metasurface consists of 16 circular patches forming a 4×4 array. A rectangular cross-slot is etched at the center of the circular metal patch to improve the antenna's port isolation. In addition, the antenna's feedline employs a T-shaped microstrip line combining a rectangle and a trapezoid, which is integrated with the radiating patch to im-

prove the antenna's impedance matching. Finally, the dielectric substrate material used for the antenna is only FR4, which greatly simplifies the antenna structure, allowing the antenna to be fabricated using the printed circuit board method, facilitating mass production and easy promotion.

Acknowledgments

This work is supported partly by the Project of State Key Laboratory of Millimeter Waves under Contract of K202414, and partly by the National Natural Science Foundation of China under Contract of 62171169.

References

- [1] CHEN, C. A single-layer single-patch dual-polarized high-gain cross-shaped microstrip patch antenna. *IEEE Antennas and Wireless Propagation Letters*, 2023, vol. 22, no. 10, p. 2417–2421. DOI: 10.1109/LAWP.2023.3289861
- [2] KEDZE, K. E., WANG, H., I, PARK, I. A metasurface-based wide-bandwidth and high-gain circularly polarized patch antenna. *IEEE Transactions on Antennas and Propagation*, 2022, vol. 70, no. 1, p. 732–737. DOI: 10.1109/TAP.2021.3098574
- [3] CHEN, Z., TIAN, J., LIU, H., et al. Novel pattern-diverse millimeter-wave antenna with broadband, high-gain, enhancedcoverage for energy-efficient unmanned aerial vehicle. *IEEE Transactions on Vehicular Technology*, 2021, vol. 70, no. 5, p. 4081–4087. DOI: 10.1109/TVT.2021.3071483
- [4] GUO, J., LIU, F, ZHAO, L., et al. A dual-polarized patch antenna with high isolation. In 2019 International Symposium on Antennas and Propagation (ISAP). Xi'an (China), 2019, p. 1–3.
- [5] WANG, Z., LIU, J., LONG, Y. A simple wide-bandwidth and highgain microstrip patch antenna with both sides shorted. *IEEE Antennas and Wireless Propagation Letters*, 2019, vol. 18, no. 6, p. 1144–1148. DOI: 10.1109/LAWP.2019.2911045
- [6] TA, S. X., PARK, I. Compact wideband circularly polarized patch antenna array using metasurface. *IEEE Antennas and Wireless Propagation Letters*, 2017, vol. 16, p. 1932–1936. DOI: 10.1109/LAWP.2017.2689161
- [7] CAO, Y., CAI, Y., CAO, W., et al. Broadband and high-gain microstrip patch antenna loaded with parasitic mushroom-type structure. *IEEE Antennas and Wireless Propagation Letters*, 2019, vol. 18, no. 7, p. 1405–1409. DOI: 10.1109/LAWP.2019.2917909
- [8] LIU, W., CHEN, Z. N., QING, X. Metamaterial-based low-profile broadband aperture-coupled grid-slotted patch antenna. *IEEE Transactions on Antennas and Propagation*, 2015, vol. 63, no. 7, p. 3325–3329. DOI: 10.1109/TAP.2015.2429741
- [9] LIU, W., CHEN, Z. N., QING, X. Metamaterial-based low-profile broadband mushroom antenna. *IEEE Transactions on Antennas and Propagation*, 2014, vol. 62, no. 3, p. 1165–1172. DOI: 10.1109/TAP.2013.2293788
- [10] HUSSAIN, N., JEONG, M. J., PARK, J., et al. A broadband circularly polarized Fabry-Perot resonant antenna using a singlelayered PRS for 5G MIMO applications. *IEEE Access*, 2019, vol. 7, p. 42897–42907. DOI: 10.1109/ACCESS.2019.2908441
- [11] LIU, Z. G., LU, W. B. Low-profile design of broadband high gain circularly polarized Fabry-Perot resonator antenna and its array with linearly polarized feed. *IEEE Access*, 2017, vol. 5, p. 7164–7172. DOI: 10.1109/ACCESS.2017.2675378

- [12] SARIN, V. P., NISHAMOL, M. S, TONY, D., et al. A wideband stacked offset microstrip antenna with improved gain and low cross polarization. *IEEE Transactions on Antennas and Propagation*, 2011, vol. 59, no. 4, p. 1376–1379. DOI: 10.1109/TAP.2011.2109362
- [13] WI, S. H., LEE, Y. S., YOOK, J.-G. Wideband microstrip patch antenna with u-shaped parasitic elements. *IEEE Transactions on Antennas and Propagation*, 2007, vol. 55, no. 4, p. 1196–1199. DOI: 10.1109/TAP.2007.893427
- [14] SHAFAI, L. Slotted microstrip patch antenna and its influence on wideband planar antenna designs. In 2020 IEEE Asia-Pacific Microwave Conference (APMC). Hong Kong, 2020, p. 360–362. DOI: 10.1109/APMC47863.2020.9331537
- [15] DAS, A., MOHANTY, M. N., MISHRA, R. K. Optimized design of H-slot antenna for bandwidth improvement. In 2015 IEEE Power, Communication and Information Technology Conference (PCITC). Bhubaneswar (India), 2015, p. 563–567. DOI: 10.1109/PCITC.2015.7438228
- [16] GUO, Y. X., LUK, K. M., LEE, K. F. Broadband dual polarization patch element for cellular-phone base stations. *IEEE Transactions* on Antennas and Propagation, 2002, vol. 50, no. 2, p. 251–253. DOI: 10.1109/8.998004
- [17] MAK, K. M., LAI, H. W., LUK, K. M. Wideband dual polarized antenna fed by L- and M-probe. In 2012 Asia Pacific Microwave Conference Proceedings. Kaohsiung (Taiwan), 2012, p. 1058 to 1060. DOI: 10.1109/APMC.2012.6421824
- [18] LAI, H. W., LUK, K. M. Dual polarized patch antenna fed by meandering probes. *IEEE Transactions on Antennas and Propagation*, 2007, vol. 55, no. 9, p. 2625–2627. DOI: 10.1109/TAP.2007.904158
- [19] MOSALLAEI, H., SARABANDI, K. Antenna miniaturization and bandwidth enhancement using a reactive impedance substrate. *IEEE Transactions on Antennas and Propagation*, 2004, vol. 52, no. 9, p. 2403–2414. DOI: 10.1109/TAP.2004.834135
- [20] COSTA, F., LUUKKONEN, O., SIMOVSKI, C. R., et al. TE surface wave resonances on high-impedance surface based antennas: Analysis and modeling. *IEEE Transactions on Antennas* and Propagation, 2011, vol. 59, no. 10, p. 3588–3596. DOI: 10.1109/TAP.2011.2163750
- [21] WU, B., JI, P., LI, Y., et al. A microstrip antenna achieves dual polarization conversion by rotating metasurface. *IEEE Access*, 2024, vol. 12, p. 121387–121394. DOI: 10.1109/ACCESS.2024.3452974
- [22] HE, Y., LI, Y., SUN, W., et al. Dual linearly polarized microstrip antenna using a slot-loaded TM₅₀ mode. *IEEE Antennas and Wireless Propagation Letters*, 2018, vol. 17, no. 12, p. 2344–2348. DOI: 10.1109/LAWP.2018.2874472

- [23] AFSHANI, A., WU, K. Dual-polarized patch antenna excited concurrently by a dual-mode substrate integrated waveguide. *IEEE Transactions on Antennas and Propagation*, 2022, vol. 70, no. 3, p. 2322–2327. DOI: 10.1109/TAP.2021.3118816
- [24] LUO, Y., CHEN, Z. N., MA, K. A single-layer dual-polarized differentially fed patch antenna with enhanced gain and bandwidth operating at dual compressed high-order modes using characteristic mode analysis. *IEEE Transactions on Antennas and Propagation*. 2020, vol. 68, no. 5, p. 4082–4087. DOI: 10.1109/TAP.2019.2951536

About the Authors ...

Xiwang DAI was born in Caoxian, Shandong, China. He received the B.S. and M.S. degrees in Electronic Engineering from Xidian University, Xi'an, Shaanxi, China, in 2005 and 2008. And he received Ph.D degree of Electromagnetic Fields and Microwave Technology at Xidian University in 2014. From March 2008 to August 2011, he worked at Guangdong Huisu Corporation as a manager of antenna department. Now, he is working at the Hangzhou Dianzi University, Hangzhou, China. His current research interests involve broadband antenna, RCS and metasurface.

Junshi ZHAO was born in Zhoukou, Henan, China. He received the B.S. degree in Electronic Information Engineering from the Xi'an Shiyou University, Xi'an, Shanxi, in 2023. He is currently pursuing the master's degree with Hangzhou Dianzi University, Hangzhou, Zhejiang, China. His current research interests include broadband antenna and microstrip antenna.

Gang LI (corresponding author) was born in Suizhou, Hubei, China. He received the B.S. degrees in Electronic Engineering from Xidian University, Xi'an, Shaanxi, China, in 2005. And he received Ph.D. degree of Electromagnetic Fields and Microwave Technology at Xidian University in 2009. From May 2010 to August 2012, he worked at Huawei Technologies Co., Ltd. as an EMC Engineer. Now, he is working at Hubei University of Arts and Science, Xiangyang, China. His current research interests involve broadband antenna, RCS and metasurface.